Hard X-ray Emission by Resonant Compton Upscattering in Magnetars

Zorawar Wadiasingh & Matthew G. Baring
Rice University
Peter L. Gonthier
Hope College

Texas Symposium 2013
December 9, 2013

Magnetars: Pulsars with B ~ 10^{14} G

- Standard vacuum rotating dipole model allows for an estimate of the surface magnetic field;
- SGRs and AXPs are not rotation-powered — particle acceleration and emission must ultimately derive from energy stored in the magnetic field.

$$B_0 = \left(\frac{3Ic^3 P\dot{P}}{2\pi^2 R^6} \right)^{1/2}$$

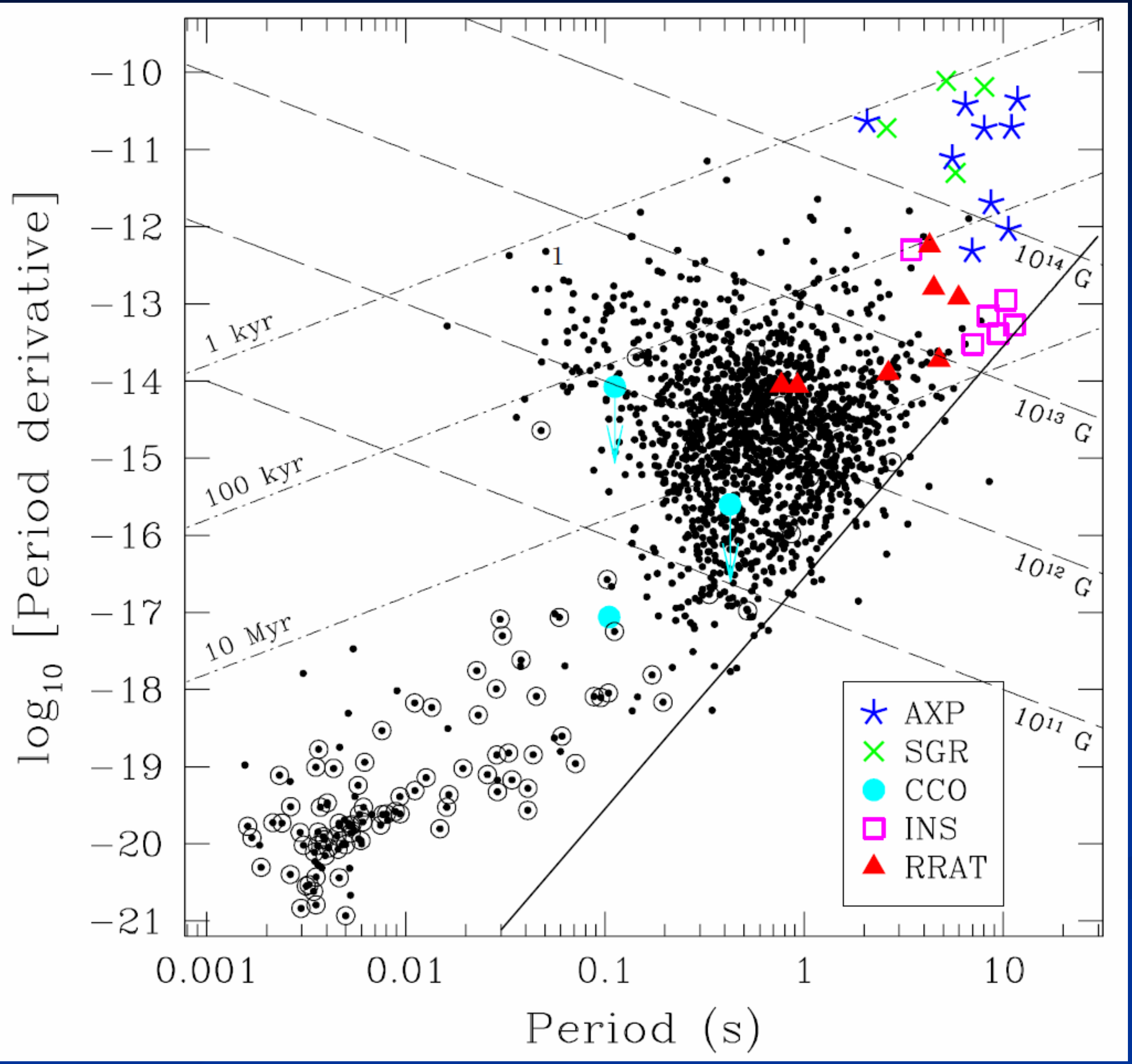

Kaspi 2010

INTEGRAL/RXTE Spectrum for AXP 1RXJS J1708-4009

- XMM spectrum below 10 keV dominates pulsed RXTE/PCA spectrum (black crosses);
- RXTE-PCA (blue) + RXTE-HEXTE (acqua) and INTEGRAL-ISGRI (red) spectrum in 20-150 keV band *is not totally pulsed,* with E^{-1}.
- COMPTEL upper limits *imply spectral turnover around 300-500 keV*, indicated by logparabolic guide curve.

Den Hartog et al. (2008)

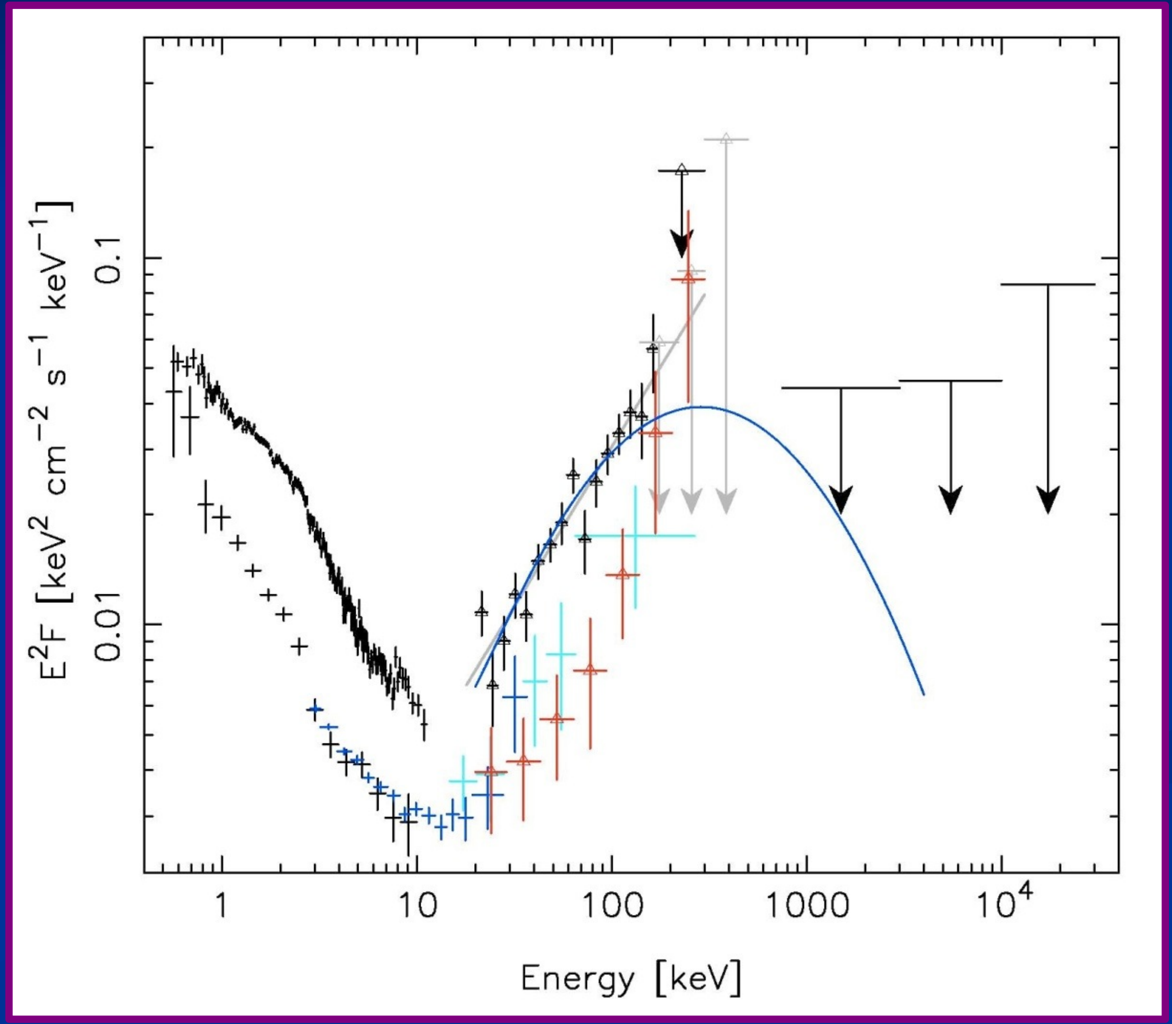

Resonant Compton Cross Section (ERF)

B = 1 => B = 4.41 x 10^{13} G

Gonthier et al. 2000

- Illustrated for photon propagation along B and the Johnson & Lipmann formalism;
- In magnetar fields, cross section declines due to Klein-Nishina reductions;
- Resonance at cyclotron frequency eB/m_ec;
- Below resonance, *l=0* provides contribution;
- In resonance, cyclotron decay width truncates divergence.

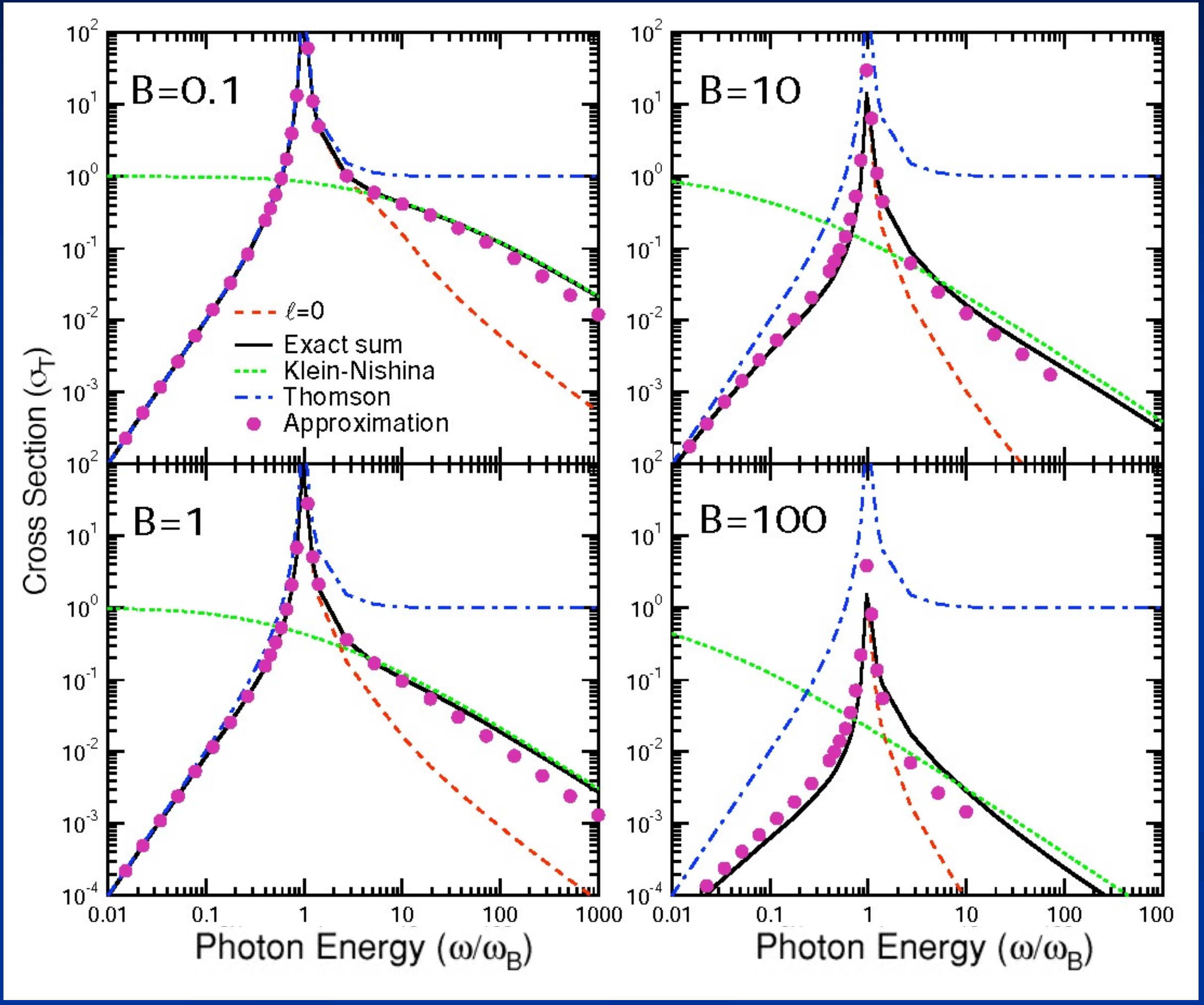

Compton Upscattering Spectrum: Uniform B

Baring & Harding 2007

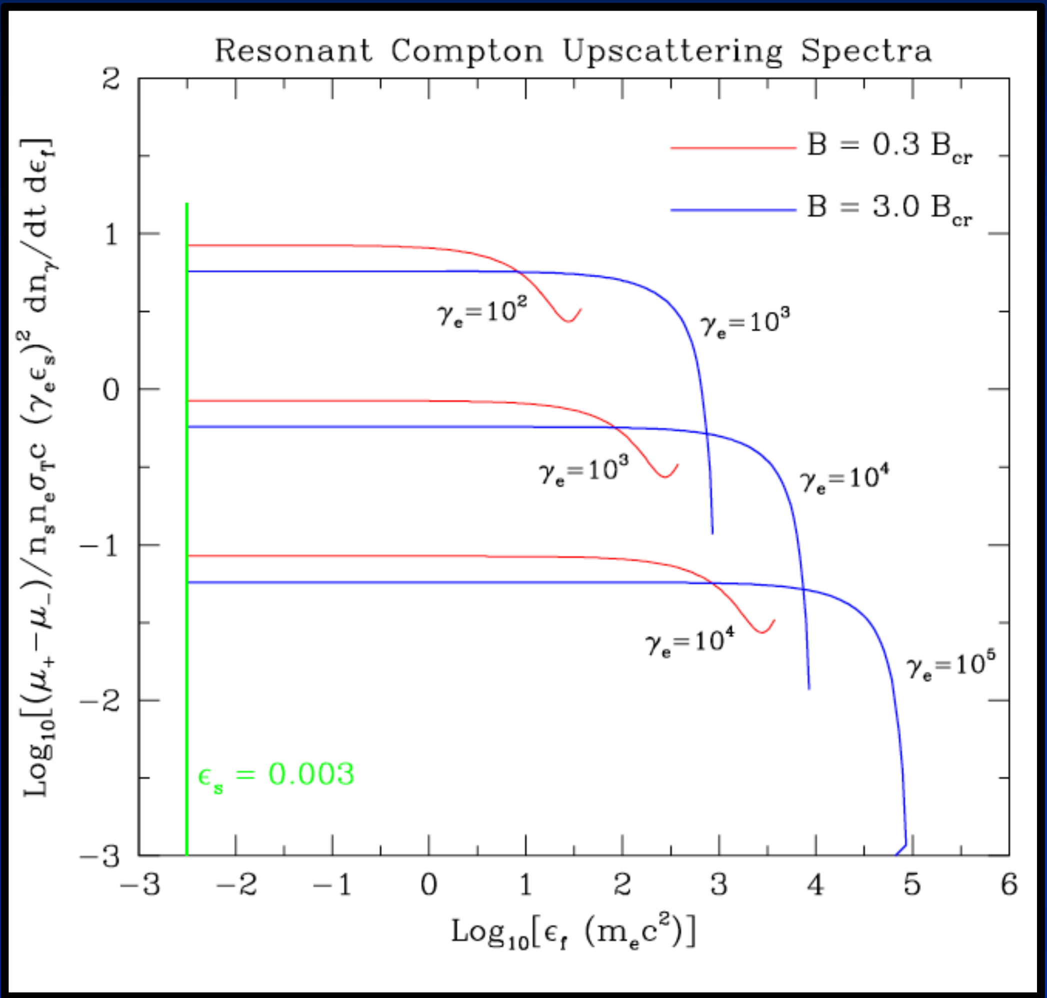

- Uniform B, monoenergetic surface X-ray seed photons;
- Resonance is sampled kinematically, leading to flat-top distributions (e.g. Dermer 1990);
- One-to-one coupling between scattering angle and final energy;
- Beaming of energy along B;
- In pulsar geometry, this translates to *broader pulse profiles* and emission at lower energies, on average, *off the magnetic axis*.

$$\gamma\varepsilon_i(1-\beta\cos\theta_{kB,i}) \approx B \sim \gamma\varepsilon_f(1-\beta\cos\theta_{kB,f})$$

High B Resonant Compton Cooling

Baring, Wadiasingh & Gonthier 2011

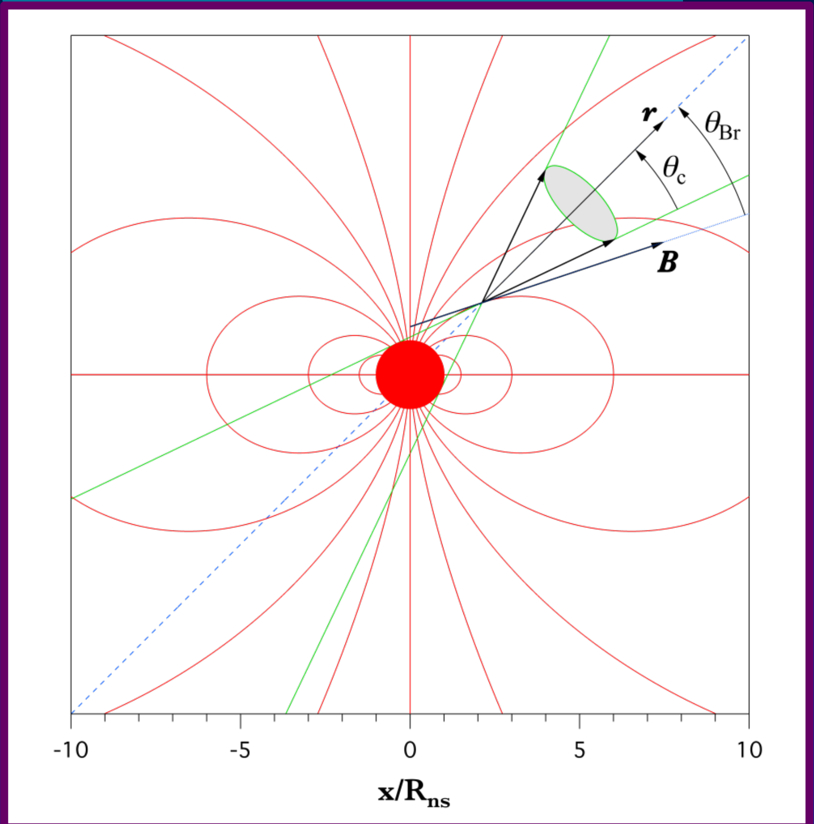

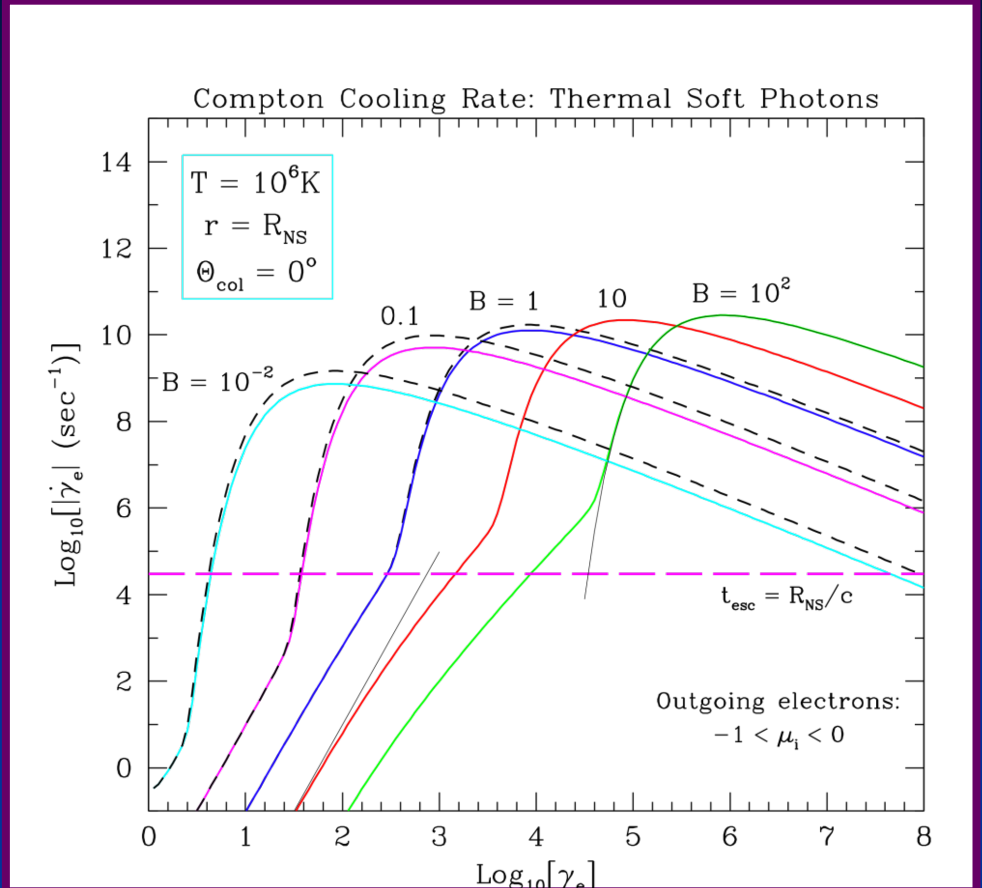

- **Resonant cooling is strong for all Lorentz factors γ above the kinematic threshold for its accessibility; magnetic field dependence as a function of B is displayed at the *right* (dashed lines denote JL spin-averaged calculations, instead of the spin-dependent ST cross section).**
- **Kinematics dictate the B dependence of the cooling rate at the Planckian maximum. For magnetar magnetospheres, Lorentz factors following injection are limited to ~10^1-10^3 by cooling.**

Observer Perspectives and Resonant Scattering I

- For a given scattered energy ε_f (in units of m_ec^2) resonant interactions (black points, below) occur at different points long a field loop;
- The hardest emission comes from angles beaming to the observer close to backscattering in the electron rest frame for "meridional" field loops relative to the observer.

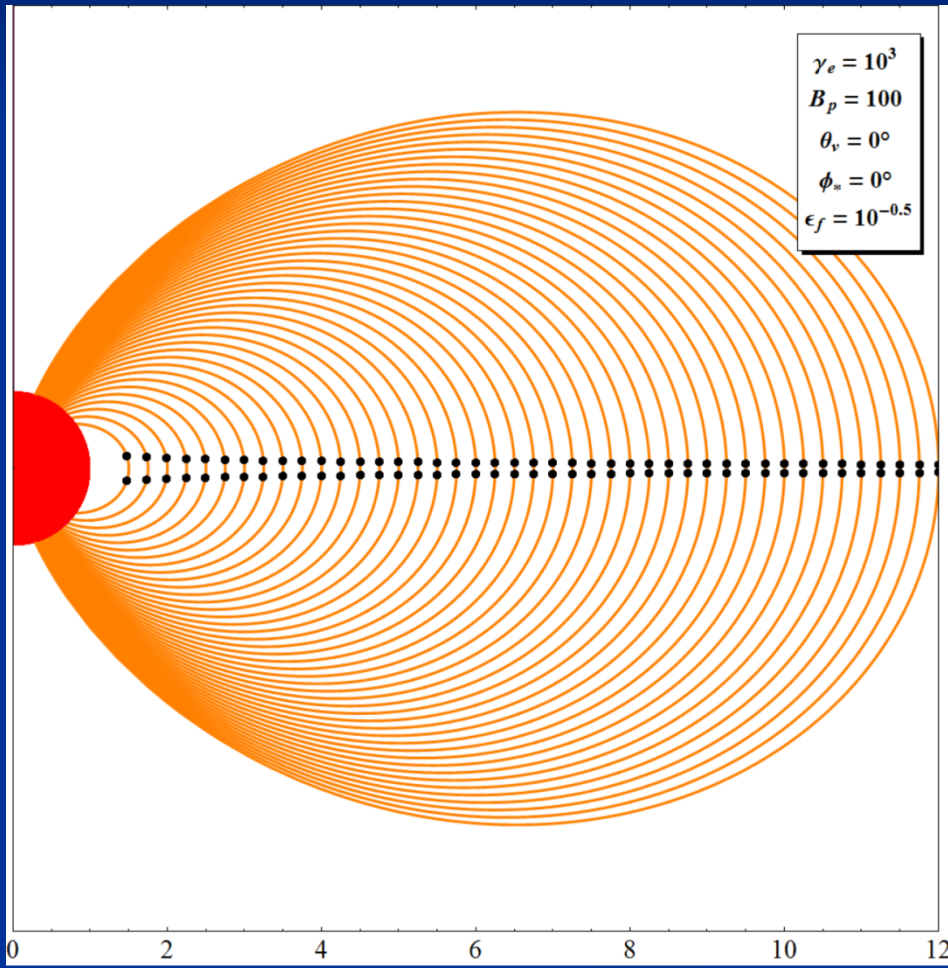

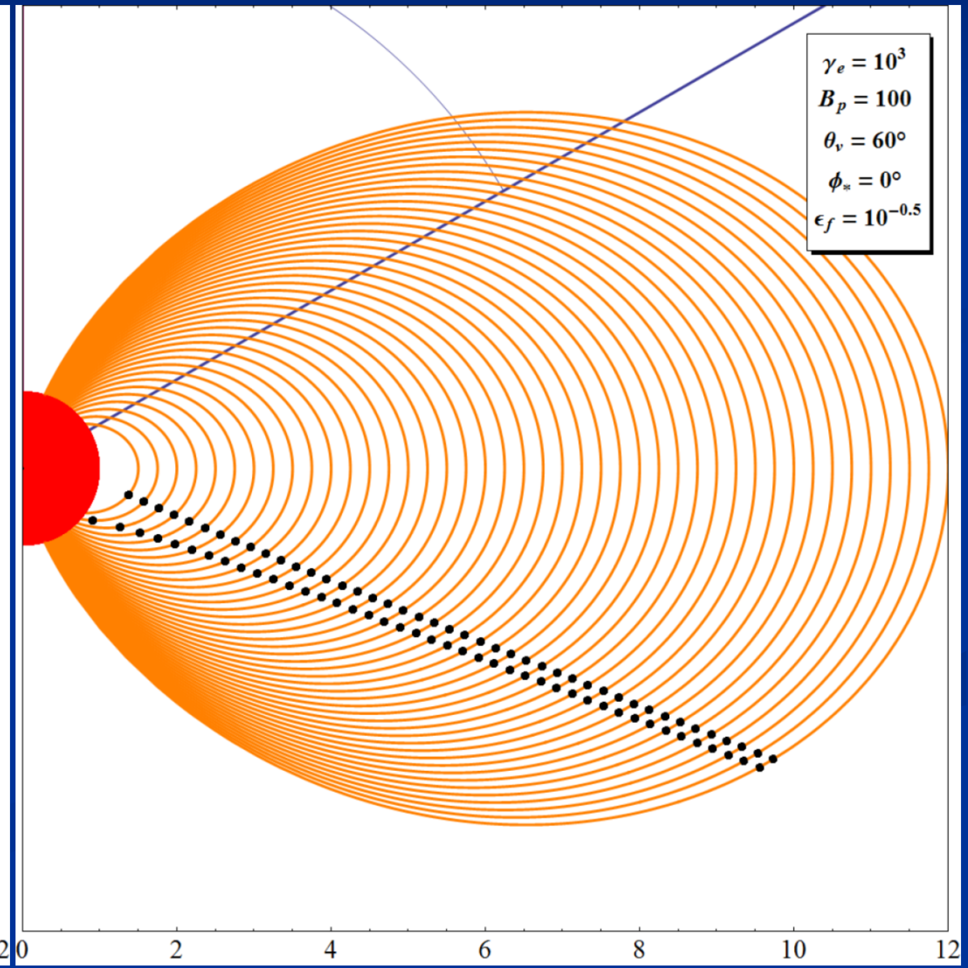

Resonant Scattering II: Orthogonal Projections

- Black points bound the locii ("green" and "blue") of final scattered energies of greater than $\varepsilon_f = 10^{-0.5}$ => 160 keV;
- For most viewing angles, this is a very small portion of the activated magnetophere for the Lorentz factor and polar field chosen below.

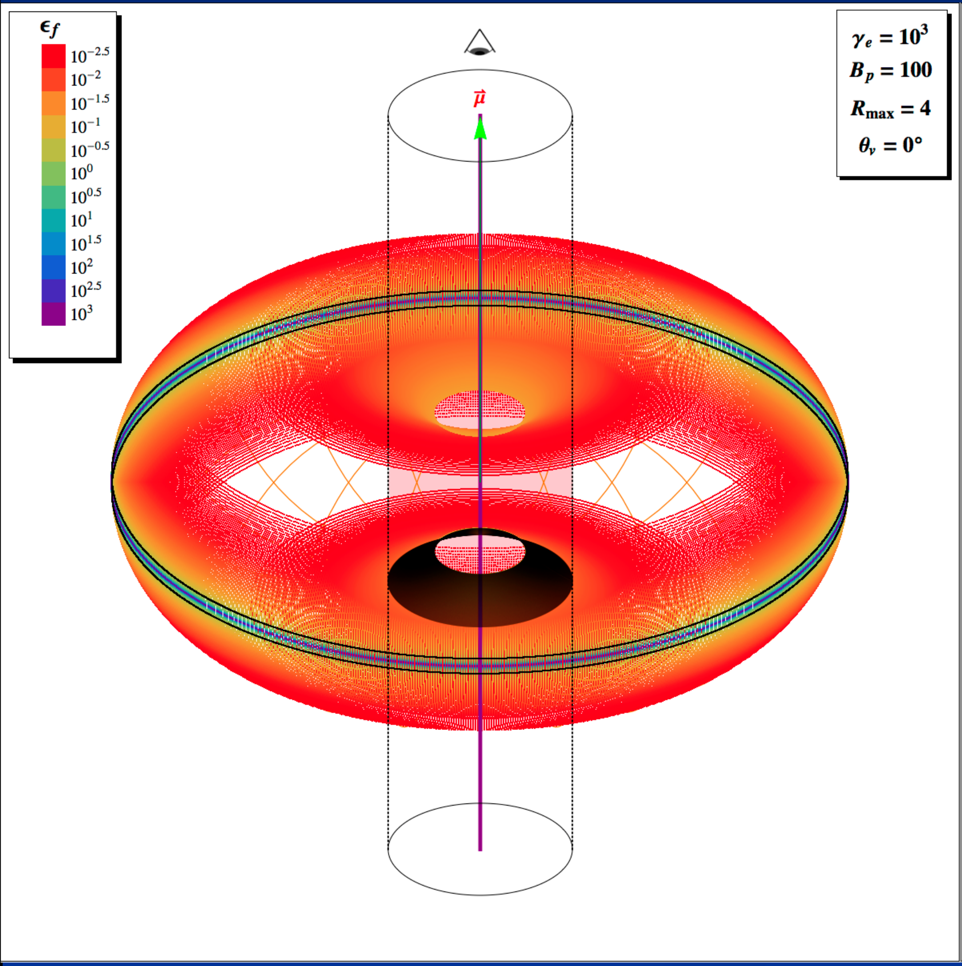

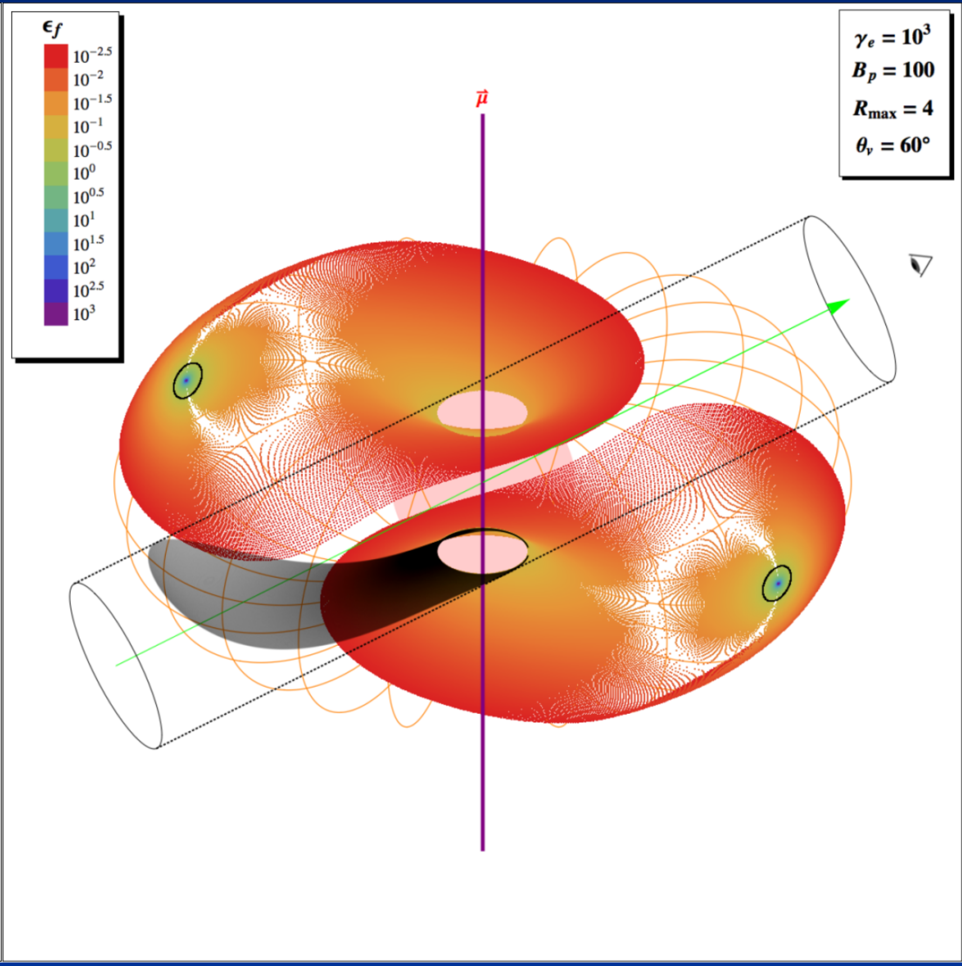

Observer Perspectives and Resonant Scattering III

- Note that **shadowing** (gray zones) may be important for some viewing angles;
- Some instantaneous viewing angles **never** sample the hardest emission.

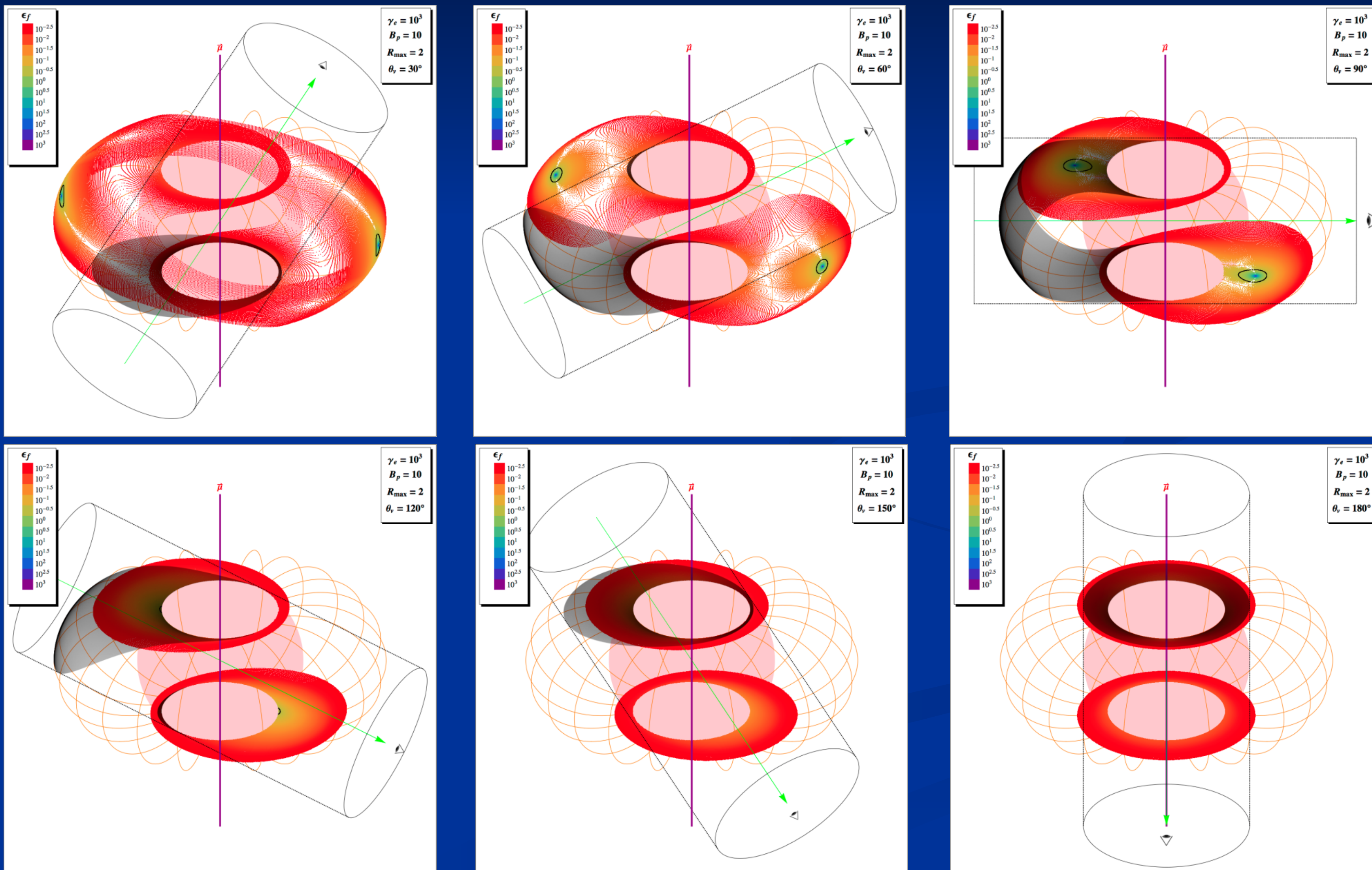

Photon Spectra Varying Lorentz Factor

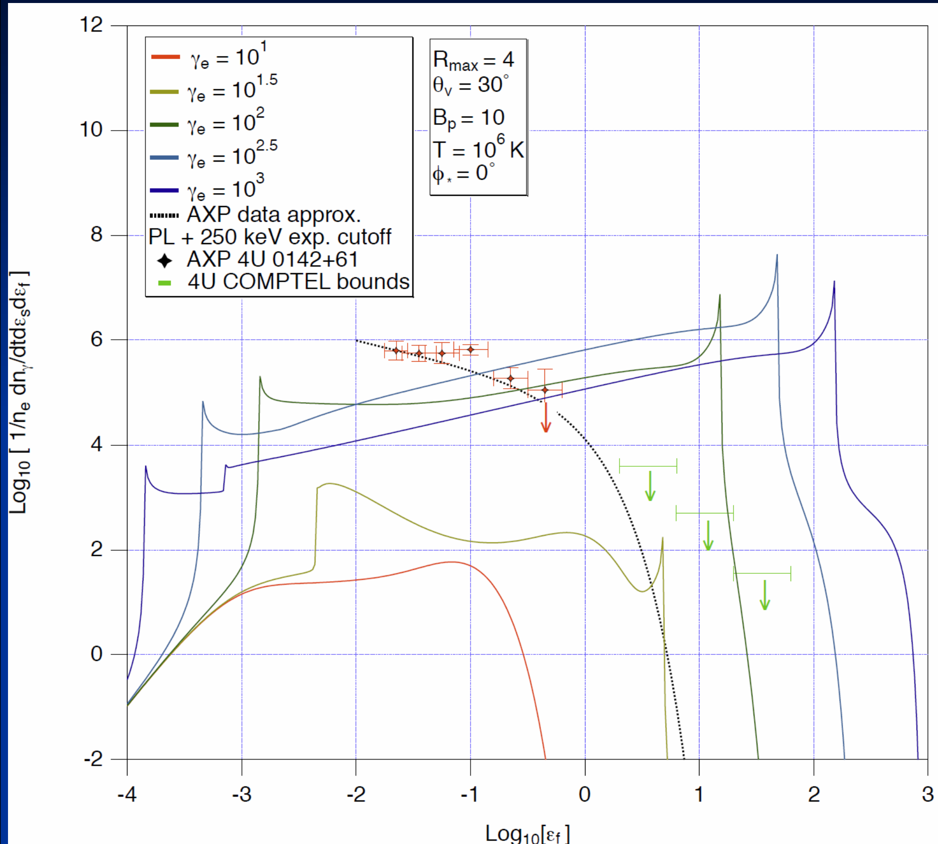

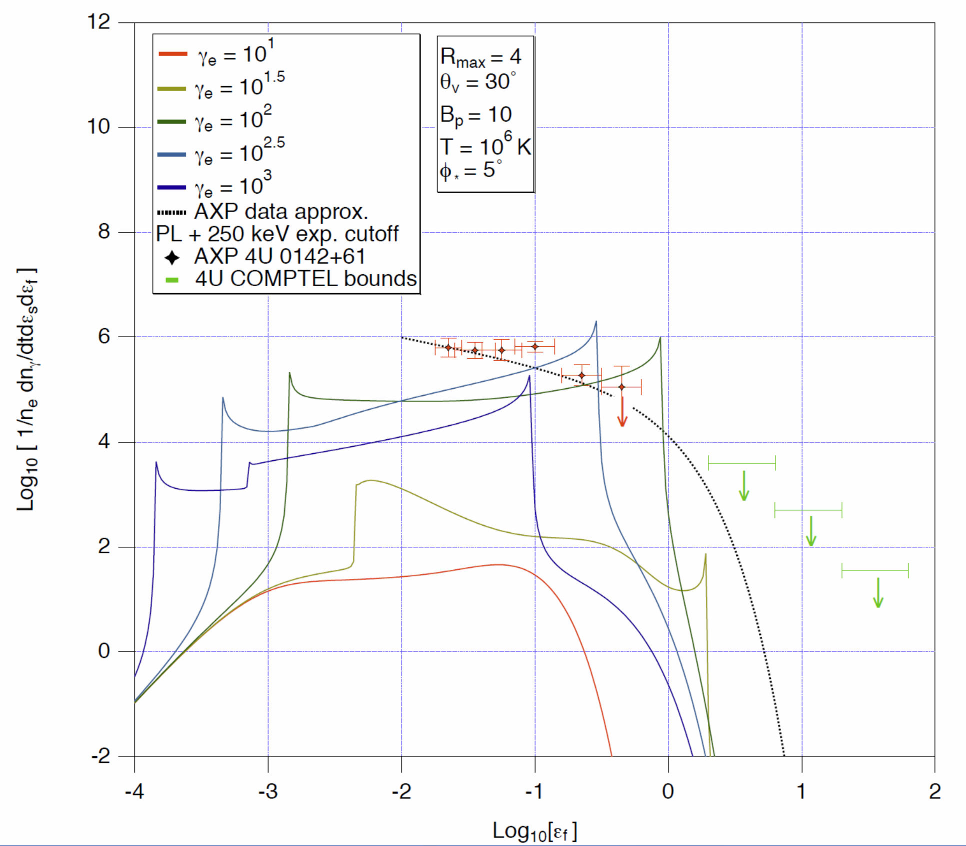

- **Resonant interactions may be sampled kinematically at multiple colatitudes**, and beamed along an observer perspective for field loops close to the "meridian" and "anti-meridian" relative to the line-of-sight;
- Power-law index E^s of s ~ 0.5 for high Lorentz factors.
- A spectrum of AXP 4U 0142+61 is overlaid with arbitrary normalization.

Photon Spectra Varying Observer Perspectives

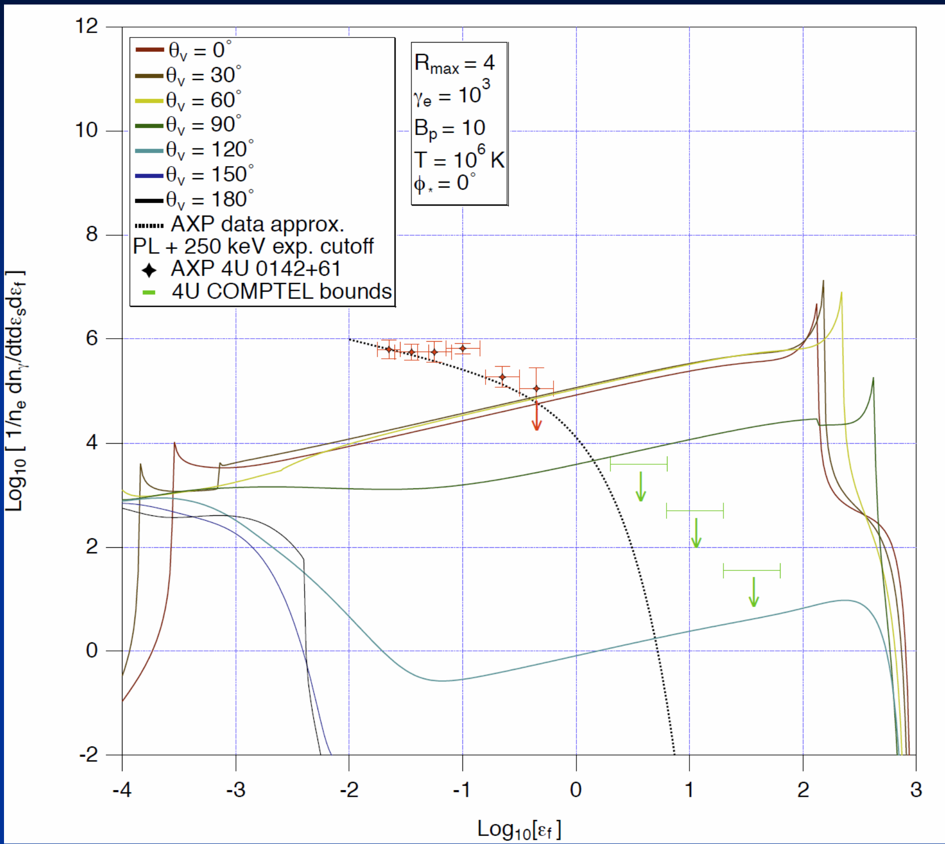

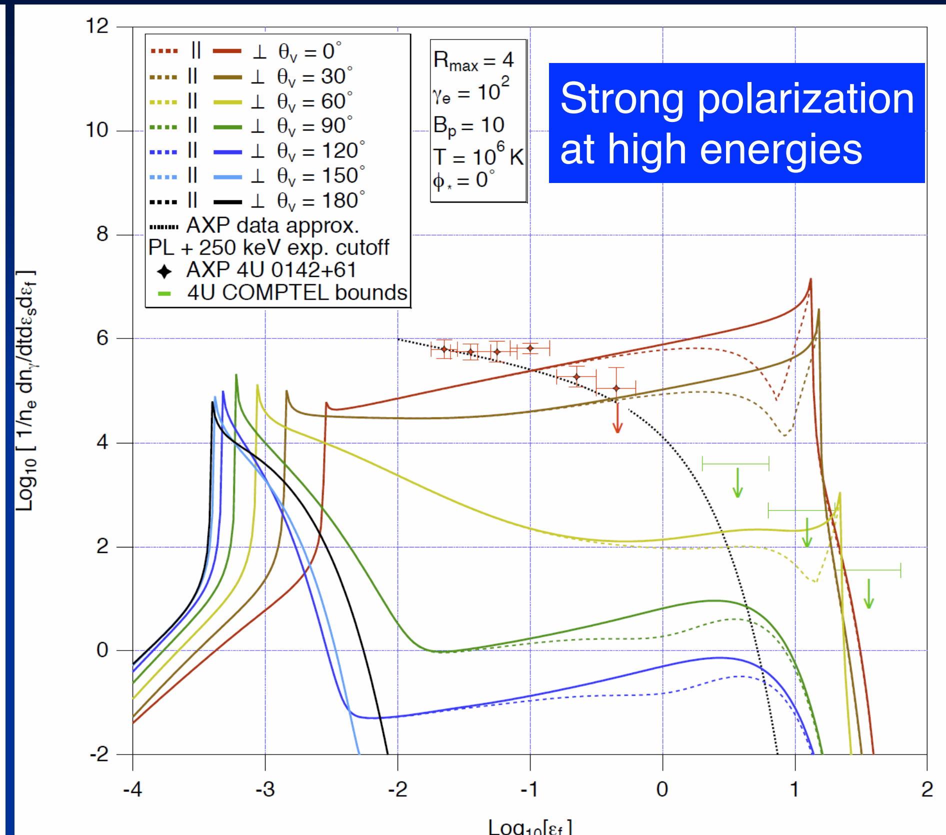

- Only a certain range of instantaneous viewing angles sample the highest final scattering angle resonant interactions for a given Lorentz factor;
- Polarization signature may be observable in a future hard X-ray mission with polarimetry.

Radiation Reaction Limited Acceleration

- Simple model of cooling, neglecting pile-up in the electron distribution, results in spectra that are similar to those of constant Lorentz factor.
- Radiation reaction limited acceleration for a uniformly activated magnetosphere introduces asymmetry in beamed Lorentz factors for meridional and anti-meridional field loops.

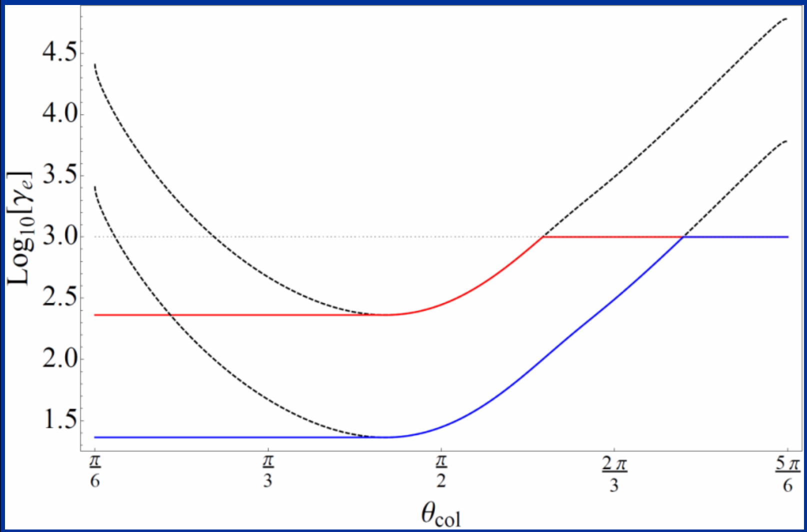

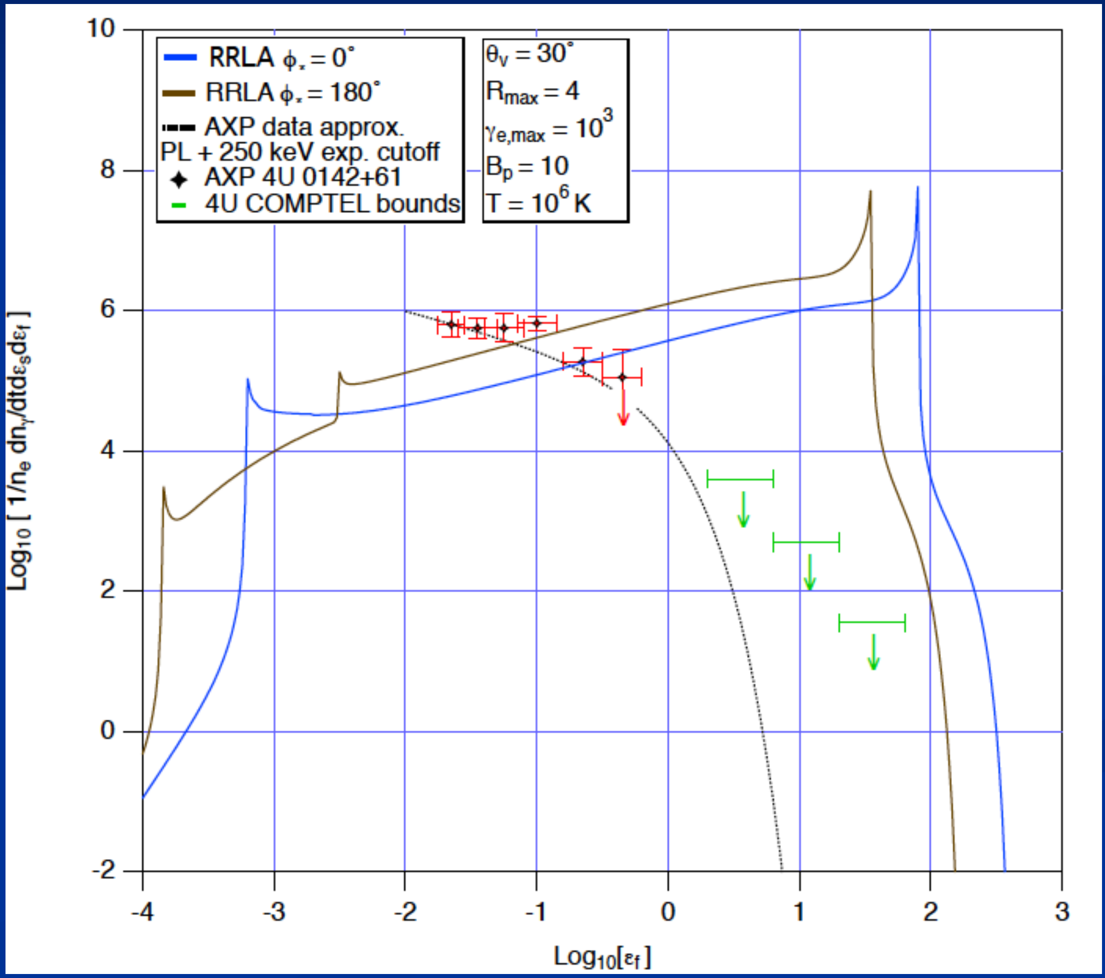

Summary

- Resonant Compton upscattering can efficiently generate flat spectra that are strongly dependent on observer perspective, electron Lorentz factor and emission locale;
- Portions of the activated magnetosphere that violate COMPTEL bounds are spatially small;
- e^- cooling and the contribution from multiple interaction locales must be incorporated to steepen the spectral index.
- Future: radiation reaction limited e^- cooling, kinetic equation analyses, output phase-resolved spectra with polarizations.

References

- Baring, M. G., Gonthier, P. L., Harding A. K. 2005, ApJ, 630, 430.
- Baring, M. G. & Harding, A. K. 2007 ApSS, 308, 109.
- Baring, M. G.. Wadiasingh Z. & Gonthier, P. L., 2011, ApJ, 733, 61.
- Blandford, R. D. & Scharlemann, E. T. 1976, MNRAS 174, 59.
- Bussard, R. W., Alexander, S. B. & Meszaros, P 1986, PRD, 34, 440.
- Canuto, V., Lodenquai, J. & Ruderman, M., 1971, PRD, 3, 2303.
- Daugherty, J. K., & Harding, A. K. 1986, ApJ, 309, 362.
- Den Hartog, P. R., et al. 2008a, A&A, 489, 245.
- Den Hartog, P. R., et al. 2008b, A&A, 489, 263.
- Dermer, C. D. 1990, ApJ, 360, 197.
- Gonthier, P. L., Harding A. K., Baring, M. G., et al. 2000, ApJ, 540, 907.
- Herold, H. 1979, PRD, 19, 2868.
- Kuiper, L., Hermsen, W., den Hartog, P. R., et al. 2006, ApJ, 645, 556.
- Kuiper, L., Hermsen, W. & Mendez, M. 2004, ApJ, 613, 1173.
- Latal, H. G. 1986, ApJ, 309, 372.
- Pavlov, G. G. et al. 1991, ApJ, 380, 541.
- Nobili, F., et al. 2008, MNRAS, 389, 989.
- Sturner, S. 1995, ApJ 446, 292.
- Thompson, C. & Beloborodov, A. M. 2005, ApJ, 634, 565.

Observer Perspectives: Kinematics & Geometry

- Technique: invert kinetic relations between initial and final photon energies;
- Viewing perspective fixes the final scattering angle Θ_{Bn} or θ_f;
- Integrate over all colatitudes along a field line for a given instantaneous observer perspective;
- Only certain values of ε_f and θ_{col} are kinematically allowed for a given thermal seed photon energy (restrictions are imposed via an angular distribution function).
- Right: selection of resonant interactions (black points) as a function of field loop colatitude for a given final scattered energy (color coding).

$$\omega_i = \frac{\omega_f(2 - \omega_f + \omega_f \cos^2\theta_f)}{2(1 - \omega_f + \omega_f \cos\theta_f)}$$

$$\omega_f = \gamma_e \epsilon_f (1 + \beta_e \cos\Theta_{Bn})$$

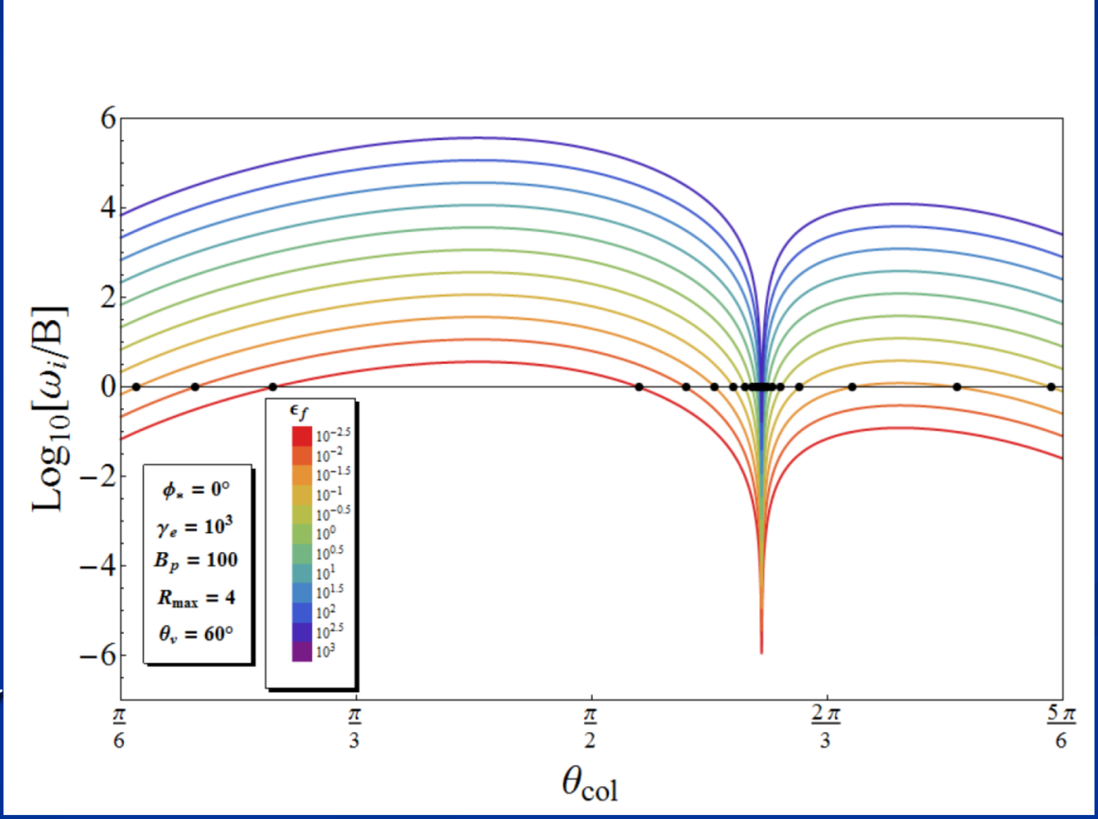

High Bp

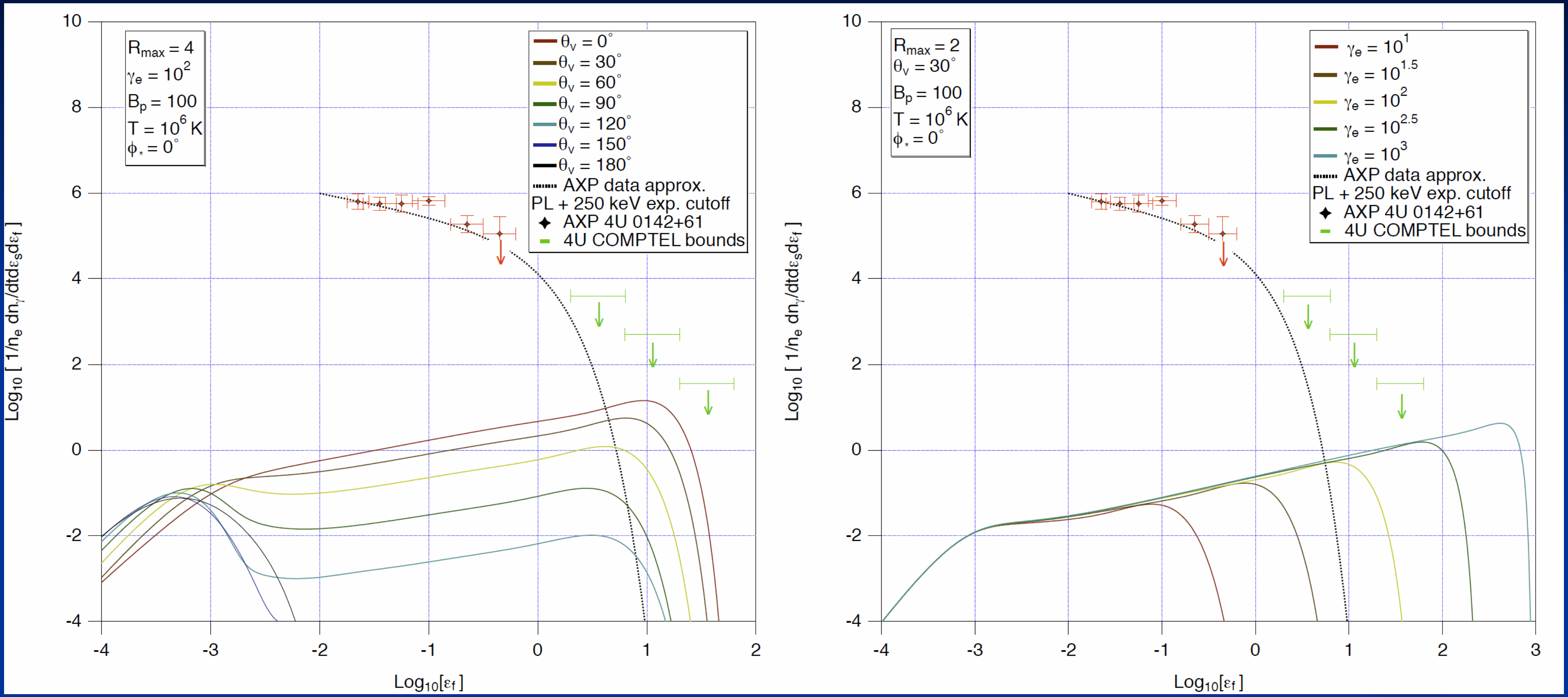

- At high local B, Lorentz factors of even 10^3 are not high enough to sample the full Wien peak of the thermal spectrum. Thus the spectra are muted, with resonant interactions sampling the Wien tail of incoming photons.

Photon Spectra Varying Lorentz Factor

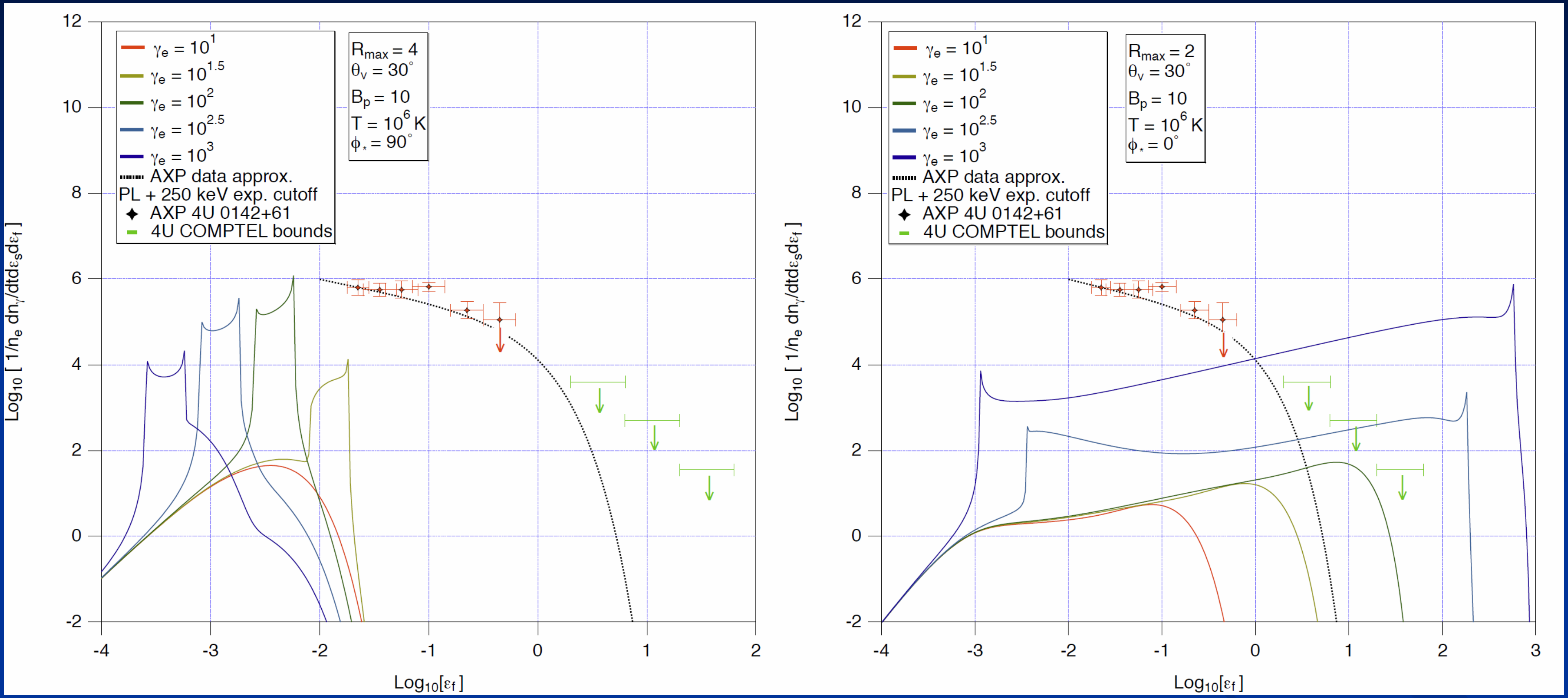

- Sampling **azimuthal field loops $\phi_* \neq 0$ relative to the line-of-sight** produce increasingly softer spectra due to softer beaming;
- Increasing B_p, or similarly decreasing R_{max} results in harder spectra only for the highest Lorentz factors where resonant interactions are sampled.

Model Setup & Directed Emission Spectra

- Electrons are accelerated along closed field loops for a dipole field geometry at a fixed Lorentz factor γ_e;
- The activated region can be a localized bundle of field loops or a full magnetosphere;
- Dipole field loops are parameterized by R_{max}, in units of neutron star radii;
- The putative acceleration is close to the neutron star surface, and for concreteness, is taken to be the southern magnetic footpoint;
- No resonant Compton electron cooling is incorporated at this time;
- The observer makes an instantaneous viewing angle θ_v with respect to the magnetic axis as a function of rotation phase;
- A thermal distribution of temperature $T = 10^6$ K (kT= 0.086 keV) is assumed for the unscattered soft photons;
- An analytic collision integral formalism (e.g. Ho & Epstein 1989, Dermer 1990) is used to compute resonant IC spectra (photon production rates, or reaction rates) integrated over the soft photon distribution and over field loops.

Compton Resonaspheres

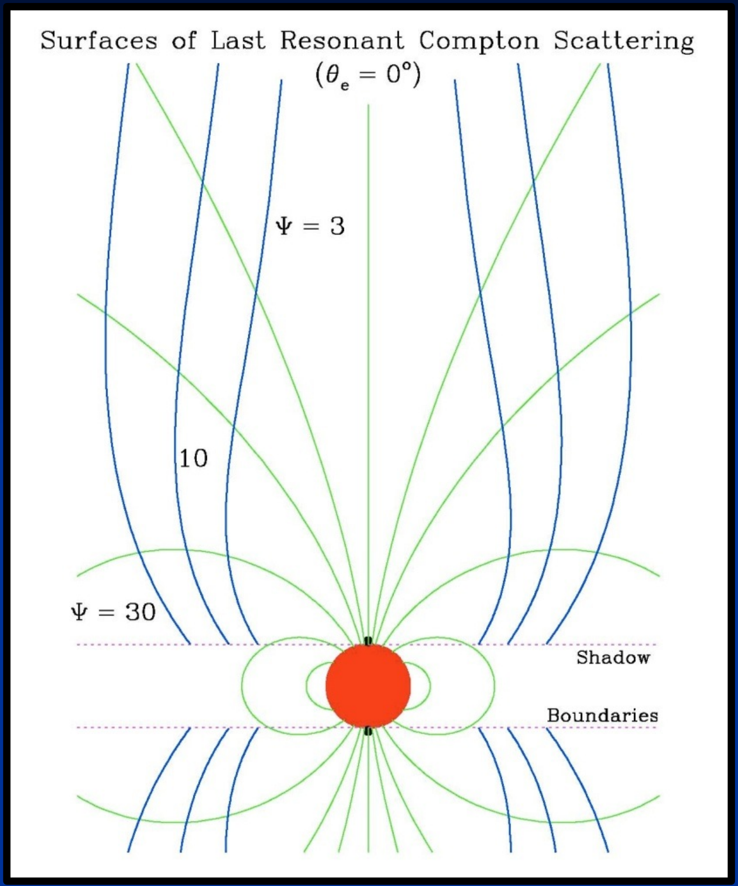

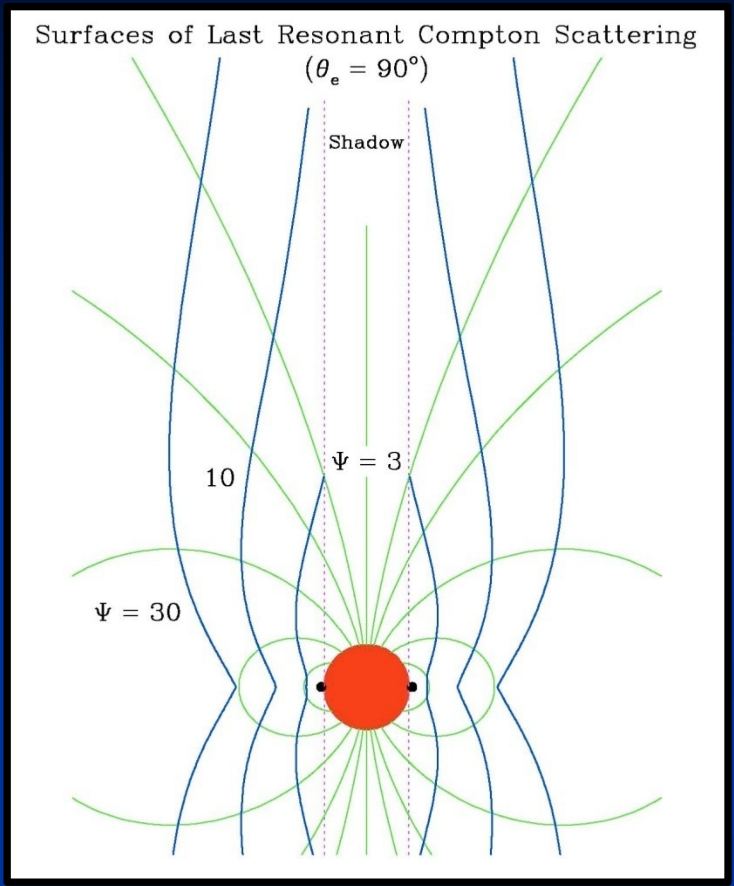

Baring & Harding 2007

- Geometrical boundaries of last resonant scattering, described in terms of the parameter $\Psi = B_p/(2\gamma_e E_\gamma)$. The black dot marks the surface emission point at colatitude θ_e. The altitude of resonance is much lower in the equatorial regions, where surface X-ray photons tend to travel more across field lines in a rotating observer's frame.

FERMI-LAT limits on 4U 0142+614

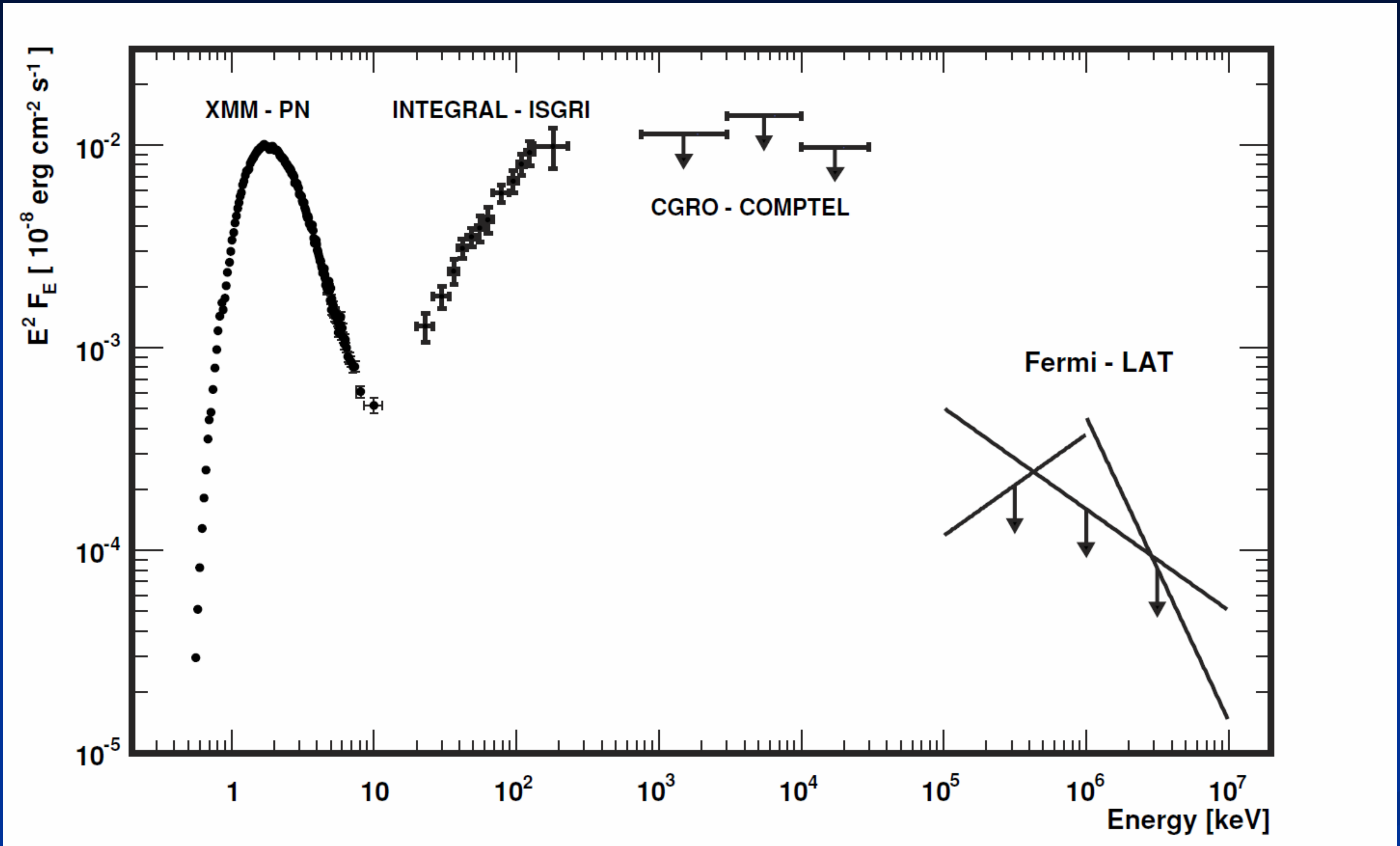

…but A. Kong et al. has reported a marginal detection (pulsations) of magnetar IE2259+586 with Fermi-LAT

Compton Upscattering Kinematics

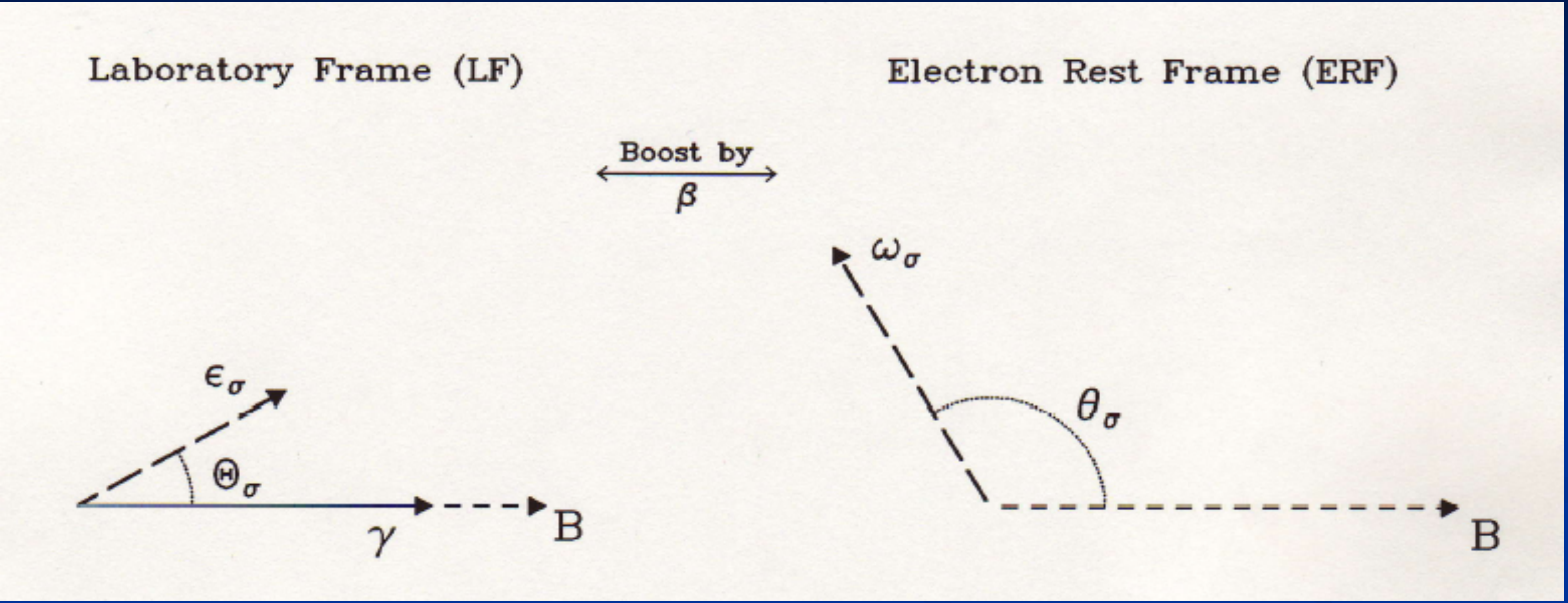

- Upscattering kinematics is often controlled by the criterion for scattering in the cyclotron resonance: there is a one-to-one correspondence between final photon angle to **B** and upscattered energy.

$$\boxed{\gamma\varepsilon_i(1-\beta\cos\theta_{kB,i}) \approx B \sim \gamma\varepsilon_f(1-\beta\cos\theta_{kB,f})}$$

Persistent Magnetars

Pulsar	SNR	P (sec)	$\dot{P}$ (sec sec^{-1})	$\tau = P/2\dot{P}$ (kyr)	B_p[b] (Gauss)	B_p/B_{cr}[c]	$\frac{L_X}{\lvert\dot{E}\rvert}$[d]	kT_b (keV)	Γ_s[e]	Γ_h[f] (total)	Γ_h^{pf} (pulsed)
SGR 1806-20[g]	–	7.60	7.5×10^{-10}	0.16	4.8×10^{15}	110	6.2	$0.6^{+0.2}_{-0.1}$	$1.6^{+0.1}_{-0.3}$	1.7 ± 0.3	–
SGR 1900+14[h]	–	5.20	9.2×10^{-11}	0.90	1.4×10^{15}	32	14	0.47 ± 0.02	1.9 ± 0.1	3.1 ± 0.5	–
AXP 1E 1841-045[i]	Kes 73	11.78	$\sim 4 \times 10^{-11}$	4.7	1.4×10^{15}	31	880	0.450 ± 0.03	1.9 ± 0.2	1.32 ± 0.11	0.72 ± 0.15
SGR 0526-66[j]	N49	8.05	3.8×10^{-11}	3.4	1.1×10^{15}	25	> 50	0.44 ± 0.02	$2.5^{+0.11}_{-0.12}$	–	–
AXP CXOU J171405.7-381031[k]	CTB 37B	3.83	$\sim 6 \times 10^{-11}$	1	9.7×10^{14}	22	> 0.75	$0.38^{+0.08}_{-0.05}$	~ 3.3	–	–
AXP 1RXS J1708-40[l]	–	11.0	1.9×10^{-11}	9.1	9.3×10^{14}	21	340	0.456 ± 0.009	$2.83^{+0.03}_{-0.08}$	1.13 ± 0.06	0.86 ± 0.16
AXP CXOU J0100-72[m]	SMC	8.02	1.88×10^{-11}	6.8	7.9×10^{14}	18	> 42	0.38 ± 0.02	2.0 ± 0.6	–	–
AXP 1E 1048.1-5937[n]	GSH 288.3-0.5-28	6.45	$\sim 2.3 \times 10^{-11}$	4.4	7.8×10^{14}	18	> 1.8	0.52	2.8	–	–
PSR J1622-4950[o]	–	4.33	1.7×10^{-11}	4.0	5.5×10^{14}	12	> 0.08	~ 0.4	–	–	–
SGR 1627-41[p]	CTB 33	2.59	1.9×10^{-11}	2.2	4.5×10^{14}	10	> 0.06	–	2.9 ± 0.8	–	–
SGR J1550-5408[q]	G327.24-0.13	2.07	2.2×10^{-11}	1.5	4.4×10^{14}	9.9	> 0.008	$0.43^{+0.03}_{-0.04}$	$3.7^{+0.8}_{-2.0}$	–	–
AXP XTE J1810-197[r]	–	5.54	7.8×10^{-12}	11	4.2×10^{14}	9.5	> 0.02	3 BB fit	–	–	–
SGR 0501+4516[s]	–	5.76	5.8×10^{-12}	16	3.7×10^{14}	8.4	–	–	–	–	–
SGR 1833-0832[t]	–	7.57	3.4×10^{-12}	35	3.3×10^{14}	7.4	–	–	–	–	–
SGR J1834.9-0846[u]	W41	2.48	8.0×10^{-12}	4.9	2.8×10^{14}	6.4	–	–	–	–	–
AXP 4U 0142+61[v]	–	8.69	2.0×10^{-12}	69	2.7×10^{14}	6.0	2900	$0.410^{+0.004}_{-0.002}$	3.88 ± 0.01	0.93 ± 0.06	0.4 ± 0.15
AXP CXOU J1647-45[w]	Westerlund 1	10.61	8.3×10^{-13}	200	1.9×10^{14}	4.3	> 10	0.49 ± 0.1	$3.5^{+1.3}_{-0.3}$	–	–
AXP 2259+586[x]	CTB 109	6.98	4.8×10^{-13}	230	1.2×10^{14}	2.7	> 390	0.412 ± 0.006	3.6 ± 0.1	–	–
SGR J1822.3-1606[y]	M17	8.44	3.1×10^{-13}	430	1.0×10^{14}	2.3	–	–	–	–	–
SGR 0418+5729[z]	–	9.08	$\sim 4 \times 10^{-15}$	3.6×10^{4}	1.2×10^{13}	0.3	~ 50	< 0.3	–	–	–

High B Magnetic Compton Physics

- Solve the Dirac equation in a static magnetic field -- there are two methods in the literature solving for the wavefunctions/ spinors/ fields: **Johnson & Lippmann** or **Sokolov & Ternov eigenstates**
- Like nonmagnetic Compton Scattering, there are two first-order Feynman diagrams:

$$[-i\gamma^{\mu}(\partial_{\mu}+iqA_{\mu})+m]\psi=0$$